



Electrochemical reduction of carbon dioxide at various series of copper single crystal electrodes

Y. Hori*, I. Takahashi, O. Koga, N. Hoshi

Department of Applied Chemistry, Faculty of Engineering, Chiba University, Yayoi-cho, Inage-ku, Chiba 263-8522, Japan

Received 9 April 2002; received in revised form 20 May 2002; accepted 20 May 2002

Abstract

Electrochemical reduction of carbon dioxide was studied with various series of copper single crystal electrodes in 0.1 M KHCO_3 aqueous solution at constant current density 5 mA cm^{-2} ; the electrodes employed are $\text{Cu(S)}-[n(100) \times (111)]$, $\text{Cu(S)}-[n(100) \times (110)]$, $\text{Cu(S)}-[n(111) \times (100)]$, $\text{Cu(S)}-[n(111) \times (111)]$ and $\text{Cu(S)}-[n(110) \times (100)]$. The electrodes based on (100) terrace surface give ethylene as the major product. The ethylene formation is further promoted by the introduction of (111) or (110) steps to the (100) basal plane. The highest C_2H_4 to CH_4 formation ratio amounts to 10 in terms of the current efficiency for the $(711) (=4(100) - (111))$ surface as compared with the value 0.2 for the (111) electrode. The $n(111) - (111)$ surfaces favor the formations of acetic acid, acetaldehyde and ethyl alcohol with the increase of the (111) step atom density. CH_4 formation at the $n(111) - (111)$ electrodes decreases with the increase of the (111) step atom density. The $n(111) - (100)$ surfaces give higher gaseous products; the major product is CH_4 with lower fraction of C_2+ compounds.

© 2003 Elsevier Science B.V. All rights reserved.

Keywords: Single crystal; Copper; CO_2 ; Electrochemical reduction; Electrocatalysis

1. Introduction

Structure sensitive reactions on heterogeneous surfaces have been studied using single crystal metal interfaces. Many studies with single crystal surfaces have been focused on gas–solid reactions [1], and limited number of electrochemical reactions have been carried out other than adsorption of anions on electrodes [2]. Electrochemical reduction of CO_2 to adsorbed CO at platinum single crystal electrodes were studied by Yeager and co-workers [3]. Our laboratory further extended the studies to high index planes of

platinum single crystal electrodes [4], and other platinum metals (Ir, Rh and Pd) [5–7]. We revealed that the electrocatalytic activity in CO_2 reduction is greatly enhanced by introduction of steps and kinks to the atomically flat surfaces such as (111) and (100).

Carbon dioxide is electrochemically reduced to methane, ethylene and alcohols at copper electrode [8,9]. Mechanism of the unique electrocatalytic property of copper has not yet been revealed. A preliminary study was communicated by Frese with regard to CH_4 formation on copper single crystals [10]. We also reported the electrochemical reduction of CO_2 at single crystal copper electrodes of low index planes. CH_4 formation is favored at $\text{Cu}(111)$ and C_2H_4 at $\text{Cu}(100)$ among low index planes [11]. Several reactions may proceed competitively at copper electrode,

* Corresponding author. Tel.: +81-43-290-3382;

fax: +81-43-290-3382.

E-mail address: hori@tc.chiba-u.ac.jp (Y. Hori).

and the electrocatalytic activity for the individual reactions may depend on the atomic configuration of the electrode surface. Thus, the product distribution in CO₂ reduction at Cu single crystal electrodes varies greatly with the crystal orientation of the electrode.

We further extended the study in order to find a good electrocatalyst in CO₂ reduction. In the course of this study, we showed that introduction of step sites to the Cu(100) basal plane leads to remarkably enhanced formation of C₂H₄ [12]. However, the reproducibility of the electrolysis was not very high at some crystal surfaces, particularly Cu(110) and the related crystal orientation electrodes. We examined the surface treatment procedures of the electrode, and successfully improved the reproducibility of the electrolysis results [13]. Using the newly established surface treatment of the electrodes, we comprehensively studied the electrochemical reduction of CO₂ at single crystal copper electrodes of various orientations. This article reports the results, comparing the electrocatalytic properties of various series of the crystal orientations in the electrochemical reduction of CO₂.

2. Experimental

Spherical copper single crystals (10 mm diameter) attached with a copper stick lead were prepared from 99.999% copper metal using a graphite crucible. After orientation of crystals by the X-ray Laue back reflection method, the surface of the electrode was polished mechanically to mirror finish with diamond paste down to 0.25 μm, then electrochemically polished in a mixture of concentrated phosphoric acid and sulfuric acid. Rinsed with 0.1 mM HClO₄ solution prepared from Merck Suprapur grade chemicals and ultrapure water from Milli Q low TOC (Millipore), the electrode was transferred to a Pyrex electrolysis cell with the electrode surface protected by a drop of 0.1 mM HClO₄. The electrode was quickly set in the electrolysis cell in 15 s according to the hanging meniscus configuration.

We previously reported the charge displacement adsorption of CO at the electrodes of poly- and single crystal copper in some electrolyte solutions [14–16]. Reproducible cyclic voltammograms are obtained, corresponding to the displacement of specifically adsorbed anion by adsorption of CO; the voltam-

mograms are characteristic of the crystal orientations which can be utilized as the fingerprint. In the present study, we thus verified the crystal orientations of the copper single crystal electrodes prior to the electrolysis on the basis of the voltammograms of the charge displacement adsorption of CO in 0.1 M K₂HPO₄ + 0.1 M KH₂PO₄ (pH 6.8) at 0 °C using as the fingerprints.

The electrolyte solution 0.1 M KHCO₃ for the electrochemical reduction of CO₂ were prepared from super pure grade chemicals (Nacalai Tesque), purified by pre-electrolysis using a Pt black cathode overnight prior to the measurements. The electrolyses were conducted at a constant current density of 5 mA cm⁻² for 1 h with CO₂ gas bubbled through the electrolyte solution continuously. CO₂ gas, of the purity higher than 99.99%, passed through an activated copper column and a silica gel column to remove trace amount of gaseous impurities. The electrolysis cell was stirred by a magnetic stirrer (ca. 260 rpm) and thermostated at 18 °C. The gas sample of the effluent CO₂ from the electrolysis cell was taken every 10 min, analyzed by gas chromatography. Soluble products were analyzed by an ion chromatograph (Toyo Soda) and a gas chromatograph-mass spectrometer (Shimadzu GC-MS-QP5050) after the electrolyses. More experimental details are published elsewhere [13].

3. Results and discussion

3.1. Voltammograms of copper single crystal electrodes

Fig. 1 shows voltammograms of the series of Cu(S)-[*n*(100) × (111)] electrodes composed of *n* atomic rows of (100) terrace and one atomic height of (111) step. Figs. 2 and 3 gives voltammograms of Cu(S)-[*n*(100) × (110)] and Cu(S)-[*n*(111) × (100)], respectively. Voltammograms from the Cu(S)-[*n*(111) × (111)] and Cu(S)-[*n*(110) × (100)] are not displayed here which were published in our previous paper [13].

The Cu(100) gives a sharp peak at -0.71 V with a small shoulder at -0.73 V as shown in Fig. 1. The Cu(311) (*n* = 2 in *n*(100) – (111)) gives a single peak at -0.82 V. The other two electrodes of Cu(S)-[*n*(100) × (111)] show the intermediate fea-

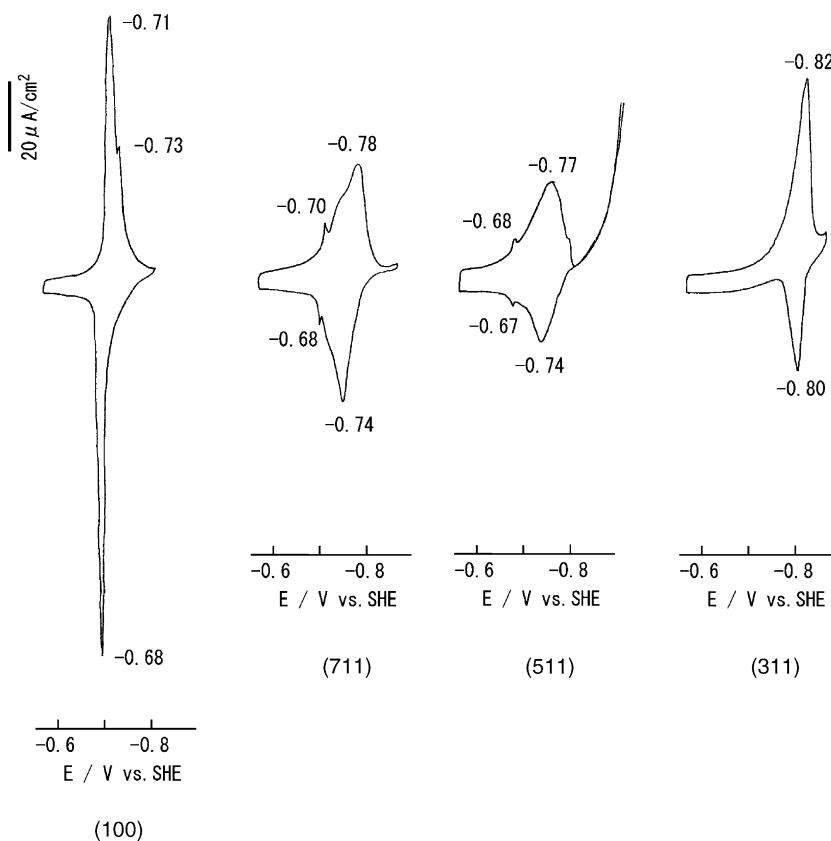


Fig. 1. Cyclic voltammograms of the Cu(S)-[$n(100) \times (111)$] electrodes obtained in CO saturated 0.1 M K_2HPO_4 + 0.1 M KH_2PO_4 (pH 6.8) at 0°C. The potentials of the peaks and shoulders are indicated.

tures between the Cu(100) and the Cu(311). With the increase of (111) step atom density or the decrease of n value, the sharp peak at -0.71 V diminishes and the broad peaks at -0.73 to -0.78 V grow.

Fig. 2 shows a series of the voltammograms of Cu(S)-[$n(100) \times (110)$]. The features of the voltammograms vary with the increase of the step atom density or the decrease of n value in a way similar to Cu(S)-[$n(100) \times (111)$] series.

Fig. 3 presents the voltammograms of Cu(S)-[$n(111) \times (100)$]. The trend is different from Figs. 1 and 2. Cu(111) does not give any peak in the measured potential range. With the increase of the step atom density, a single cathodic peak grows at -0.79 to -0.82 V, giving a couple of large redox waves at Cu(311). The cathodic peak is greater than the anodic one; the electricity of the hydrogen evolution

may be included in the redox peaks. The shape of the voltammograms of the whole series will be discussed in connection with the surface atom configuration in more detail elsewhere.

3.2. Electrolysis with electrodes of Cu(S)-[$n(100) \times (111)$] and Cu(S)-[$n(100) \times (110)$] series

The shape of the voltammograms of Cu(S)-[$n(100) \times (111)$] and Cu(S)-[$n(100) \times (110)$], measured after the electrolysis for 1 h, did not change greatly and showed identical features with those before the electrolysis. Thus, the crystal orientation of the electrodes remains stable during the electrolysis.

Table 1 demonstrates the product distributions in terms of the current efficiency together with n value. The results from the Cu(111) is added to Table 1

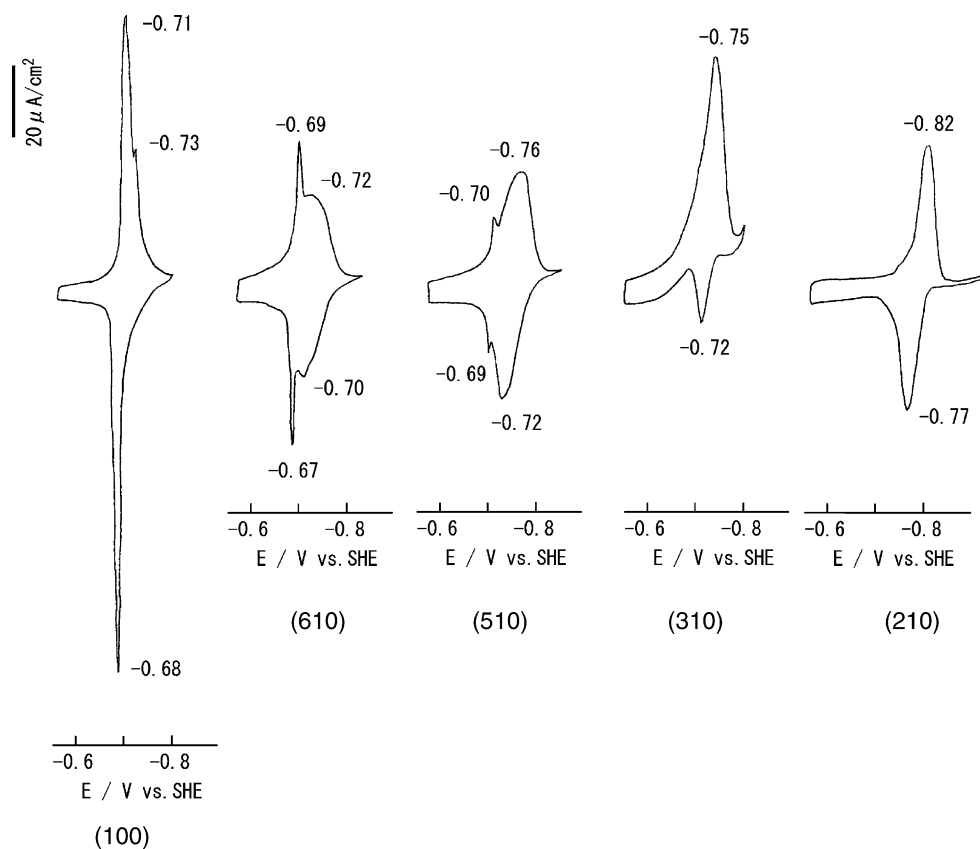


Fig. 2. Cyclic voltammograms of the Cu(S)-[$n(100) \times (110)$] electrodes obtained in CO saturated 0.1 M K_2HPO_4 + 0.1 M KH_2PO_4 (pH 6.8) at 0 °C. The potentials of the peaks and shoulders are indicated.

Table 1

Product distribution in the electrochemical reduction of CO_2 at a series of copper single crystal electrodes Cu(S)-[$n(100) \times (111)$]

Crystal orientation	n^a	Potential V vs. SHE	Current efficiency (%)												C ₂ H ₄ /CH ₄		
			CH ₄	C ₂ H ₄	CO	H ₂	MeD	EtOH	PrD	AlOH	PrOH	HCOOH	CH ₃ COOH	C ₂ +		Gas total	Total
(100)	∞	-1.40	30.4	40.4	0.9	6.8	1.6	9.7	2.8	0.8	1.5	3.0	1.0	57.8	71.7	98.9	1.3
(1111)	6	-1.37	8.9	50.2	1.8	8.8	1.1	14.4	3.3	1.0	2.3	3.2	2.1	74.4	60.9	97.2	5.6
(911)	5	-1.36	5.7	50.9	tr	12.7	1.2	16.9	2.4	2.5	4.5	3.5	1.1	79.5	56.6	101.4	8.9
(711)	4	-1.34	5.0	50.0	1.1	15.6	1.2	7.4	5.2	2.2	4.6	4.6	0.9	71.5	56.1	97.8	10.0
(511)	3	-1.36	11.4	39.0	1.9	18.1	1.4	12.2	3.0	1.6	3.3	8.8	0.8	61.3	52.3	101.5	3.4
(311)	2	-1.37	36.0	23.8	2.6	13.3	1.1	3.3	2.3	0.4	1.5	14.0	0.6	33.0	62.4	98.9	0.7
(111)	-	-1.55	46.3	8.3	6.4	16.3	2.1	2.6	0.6	0.7	0.0	11.5	1.5	15.8	61.0	96.3	0.2

Electrolyte solution: 0.1 M $KHCO_3$; current density: 5 $mA\ cm^{-2}$. MeD: acetaldehyde; EtOH: ethanol; PrD: propionaldehyde; AlOH: allyl alcohol; PrOH: propanol. C₂+ contains all the substances which have more than two carbon atoms. The gas total contains all the gaseous products other than H₂; tr: <0.05%.

^a n in Cu(S)-[$n(100) \times (111)$].

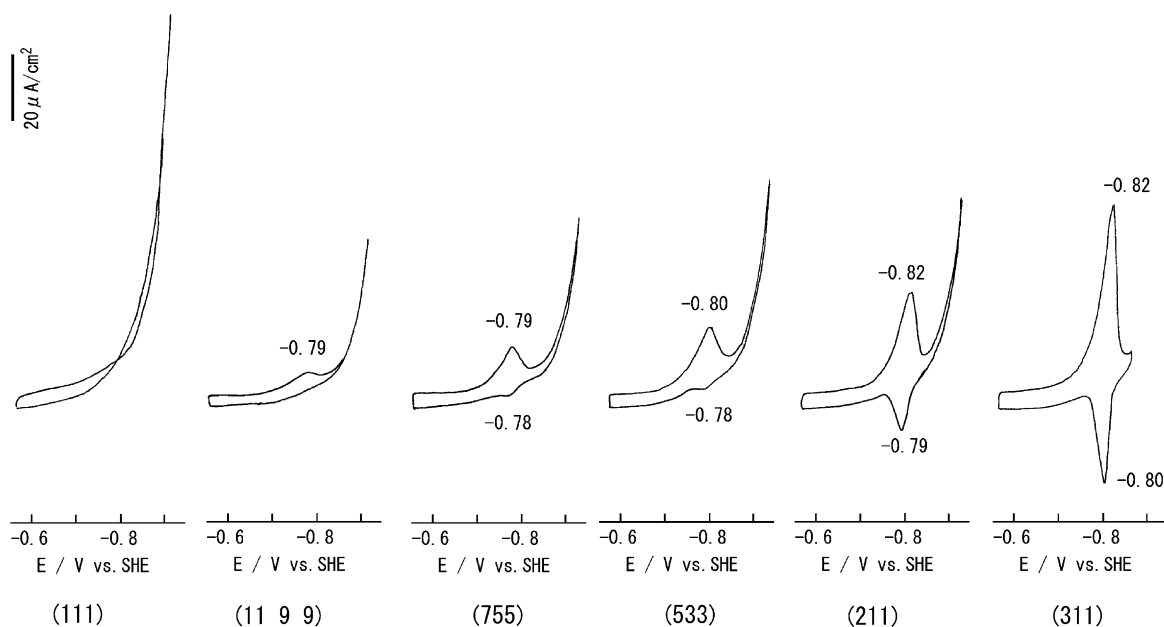


Fig. 3. Cyclic voltammograms of the Cu(S)- $[n(111) \times (100)]$ electrodes obtained in CO saturated 0.1 M K_2HPO_4 + 0.1 M KH_2PO_4 (pH 6.8) at 0 °C. The potentials of the peaks and shoulders are indicated.

for comparison. CH_4 , C_2H_4 and CO were produced as the gaseous products with small amount of H_2 . Acetaldehyde, ethanol, propionaldehyde, allyl alcohol, *n*-propanol, formic acid and acetic acid were detected as soluble products in the electrolyte solution. The total current efficiency amounted approximately to 100%. This fact verifies that the major products were accurately analyzed in the present experimental procedures.

The product distribution is significantly affected by the crystal orientation. The Cu(111) electrode gives rise to CH_4 formation with the current efficiency as high as 46% at highly negative potential. Ethylene formation on the Cu(111) remains <10%.

The Cu(100) electrode gives relatively high yield of C_2H_4 among low index planes. C_2H_4 formation increases at $n = 4$ as shown Table 1, and decreases for n below 4. C_2+ value, which contains C_2H_4 , ethanol, allyl alcohol, *n*-propanol, acetaldehyde, propionaldehyde and acetic acid, shows a similar trend with C_2H_4 . C_2+ exceeds 70% at $n = 6-4$. CH_4 formation steeply diminishes simultaneously, taking a minimum at $n = 4$. The selectivity ratio C_2H_4/CH_4 in terms of the current efficiency reaches 10 at the Cu(711). This value is 1.3 at the (100) surface, and 0.2 at the (111) sur-

face. Thus the C_2H_4/CH_4 value ranges two orders of magnitude.

Table 2 shows the results of the series Cu(S)- $[n(100) \times (110)]$, in which (100) basal plane is modified by introduction of (110) steps. The features are similar to Table 1. C_2H_4 formation once increases and then decreases with the decrease of n value; CH_4 steeply decreases and increases again. C_2H_4/CH_4 value takes 7 at $n = 8$. CH_4 formation is favorable at the Cu(210) which has the highest dangling bond density in the face centered cubic metal. It is interesting that the Cu(210) gives a product distribution similar to the Cu(111) which has the lowest dangling bond density.

Fig. 4 shows the $\log(C_2H_4)/(CH_4)$ value and the electrode potential as a function of the angle with reference to Cu(100). The $\log(C_2H_4)/(CH_4)$ value takes a maximum at (711) and (810) in $n(100) - (111)$ and $n(100) - (110)$ series, respectively. The introduction of step atoms into (100) terrace, regardless of (111) step or (110) step, promotes C_2H_4 formation, and severely suppresses CH_4 formation. Fig. 5 depicts rigid ball models for (711) and (610). The crystal orientations with similar length of (100) terrace are the most active in ethylene formation.

Table 2

Product distribution in the electrochemical reduction of CO₂ at a series of copper single crystal electrodes Cu(S)-[*n*(100) × (110)]

Crystal orientation	<i>n</i> ^a	Potential <i>V</i> vs. SHE	Current efficiency (%)														C ₂ H ₄ /CH ₄
			CH ₄	C ₂ H ₄	CO	H ₂	MeD	EtOH	PrD	AlOH	PrOH	HCOOH	CH ₃ COOH	C ₂ +	Gas total	Total	
(100)	∞	-1.40	30.4	40.4	0.9	6.8	1.6	9.7	2.8	0.8	1.5	3.0	1.0	57.8	71.7	98.9	1.3
(810)	8	-1.38	6.4	45.1	1.4	8.7	0.9	26.0	1.1	0.9	1.9	1.5	1.6	77.6	52.9	95.6	7.1
(610)	6	-1.37	7.6	44.7	0.9	9.0	1.5	26.0	1.2	1.3	2.0	1.4	1.6	78.3	53.2	97.8	5.9
(510)	5	-1.38	8.1	42.3	2.1	10.5	3.0	26.1	2.6	1.7	1.7	2.8	2.1	79.5	52.5	103.1	5.2
(310)	3	-1.42	17.7	34.6	0.0	12.8	1.7	29.9	2.6	0.9	1.9	2.7	1.6	73.2	52.3	106.4	2.0
(210)	2	-1.52	64.0	13.4	2.2	7.0	0.9	6.6	0.6	0.2	0.5	5.5	0.7	22.9	79.6	101.6	0.2

Electrolyte solution: 0.1 M KHCO₃; current density: 5 mA cm⁻². MeD: acetaldehyde; EtOH: ethanol; PrD: propionaldehyde; AlOH: allyl alcohol; PrOH: propanol. C₂+ contains all the substances which have more than two carbon atoms. The gas total contains all the gaseous products other than H₂; tr: <0.05%.

^a *n* in Cu(S)-[*n*(100) × (110)].

The electrode potentials both for Cu(S)-[*n*(100) × (111)] and Cu(S)-[*n*(100) × (110)] do not vary to a great extent, but the value takes a maximum at (711) or (610), respectively, which gives the highest C₂/C₁ value among the respective series. The electrode potential takes the most negative value at Cu(210) and Cu(111) which give high CH₄ formation.

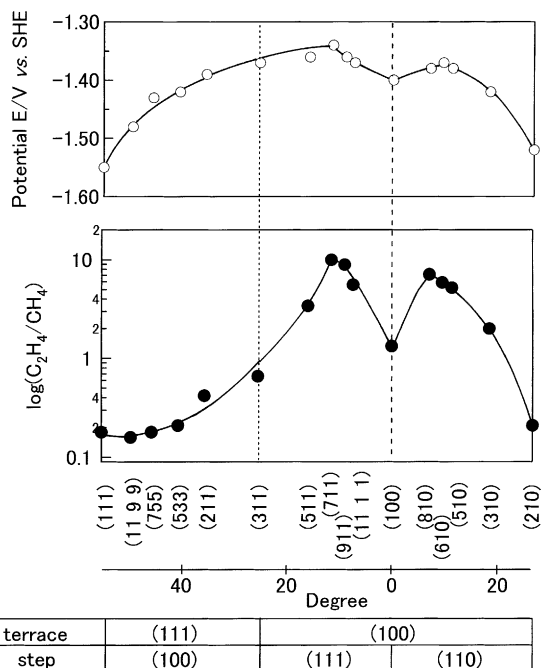


Fig. 4. Variation of log(C₂H₄/CH₄) in terms of the current efficiency and the electrode potential with the angle of the crystal orientation with the reference of Cu(100).

3.3. Electrolysis with electrodes of Cu(S)-[*n*(111) × (100)] series

The results from the Cu(S)-[*n*(111) × (100)] series is tabulated in Table 3. Introduction of (100) steps to (111) terrace does not make drastic change in the product distribution from that of the (111) electrode. The electrodes of this series are distinguished by high gaseous products and low C₂+. The formation of aldehydes, alcohols and acetic acid is very low as compared with other series of the electrodes. CH₄ formation rises and then drops with the increase of

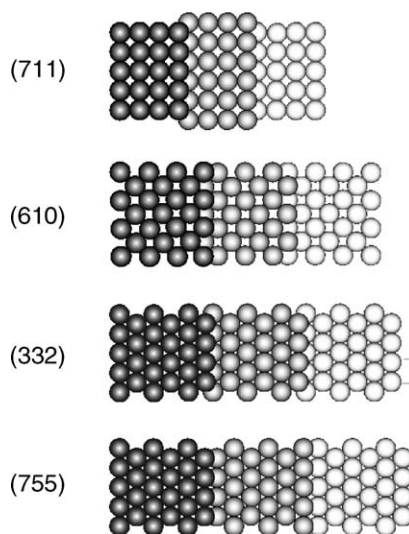


Fig. 5. Rigid sphere models of (711), (610), (332) and (755).

Table 3

Product distribution in the electrochemical reduction of CO₂ at a series of copper single crystal electrodes Cu(S)-[*n*(111) × (100)]

Crystal orientation	<i>n</i> ^a	Potential <i>V</i> vs. SHE	Current efficiency (%)														C ₂ H ₄ /CH ₄
			CH ₄	C ₂ H ₄	CO	H ₂	MeD	EtOH	PrD	AlOH	PrOH	HCOOH	CH ₃ COOH	C ₂ +	Gas total	Total	
(111)	∞	-1.55	46.3	8.3	6.4	16.3	2.1	2.6	0.6	0.7	0.0	11.5	1.5	15.8	61.0	96.3	0.2
(1199)	10	-1.48	62.4	10.2	4.9	7.2	0.5	5.9	1.6	0.0	0.2	7.9	0.8	19.2	77.5	101.6	0.2
(755)	6	-1.43	62.9	11.5	4.4	6.9	0.6	5.3	1.2	0.7	0.6	12.3	0.5	20.4	78.8	106.9	0.2
(533)	4	-1.42	62.9	13.0	3.0	4.7	0.6	1.9	0.7	0.5	0.4	9.7	0.5	17.6	78.9	97.9	0.2
(211)	3	-1.38	45.6	17.8	2.1	11.2	0.3	3.4	2.0	0.7	1.3	13.6	0.5	26.0	65.5	98.5	0.4
(311)	2	-1.37	36.0	23.8	2.6	13.3	1.1	3.3	2.3	0.4	1.5	14.0	0.6	33.0	62.4	98.9	0.7

Electrolyte solution: 0.1 M KHCO₃; current density: 5 mA cm⁻². MeD: acetaldehyde; EtOH: ethanol; PrD: propionaldehyde; AlOH: allyl alcohol; PrOH: propanol. C₂+ contains all the substances which have more than two carbon atoms. The gas total contains all the gaseous products other than H₂; tr: <0.05%.

^a *n* in Cu(S)-[*n*(111) × (100)].

the step atom density, once taking a maximum 60% at *n* = 10–4. C₂H₄ shows a gradual increase with the step atom density. The variation of log (C₂H₄)/(CH₄) is shown in Fig. 4. A rigid ball model of this series is exemplified by (755) in Fig. 5.

3.4. Electrolysis with electrodes of Cu(S)-[*n*(111) × (111)] and Cu(S)-[*n*(110) × (100)] series

The whole experimental results of the two series were published elsewhere [13]. The results from the electrodes of some selected crystal orientations are reproduced in Table 4 for the sake of comparison.

The (110) electrode is distinguished by high yields of CH₃CHO, C₂H₅OH and CH₃COOH with very low yield of CH₄. Drastic changes are remarked for CH₄, CH₃CHO, C₂H₅OH and CH₃COOH among the both crystal orientation series. C₂H₄ and HCOOH show much less variation among the two crystal orientation series.

Fig. 6 shows a correlation plot between the current efficiencies of CH₃CHO + C₂H₅OH and CH₃COOH for Cu(S)-[*n*(111) × (111)] and Cu(S)-[*n*(110) × (100)] series. This correlation suggests that CH₃CHO, C₂H₅OH and CH₃COOH may be formed from the same intermediate species.

Table 4

Product distribution in the electrochemical reduction of CO₂ at a series of copper single crystal electrodes Cu(S)-[*n*(111) × (111)] and Cu(S)-[*n*(110) × (100)]

Crystal orientation	<i>n</i>	Potential <i>V</i> vs. SHE	Current efficiency (%)														C ₂ H ₄ /CH ₄
			CH ₄	C ₂ H ₄	CO	H ₂	MeD	EtOH	PrD	AlOH	PrOH	HCOOH	CH ₃ COOH	C ₂ +	Gas total	Total	
<i>n</i> (111) – (111)																	
(111)	∞	-1.55	46.3	8.3	6.4	16.3	2.1	2.6	0.6	0.7	0.0	11.5	1.5	15.8	61.0	96.3	0.2
(332)	6	-1.51	39.6	9.9	6.1	10.3	5.1	7.1	0.2	0.3	0.2	9.4	3.4	26.2	55.6	91.6	0.3
(331)	3	-1.55	13.8	16.6	7.7	5.7	7.1	15.6	0.5	0.0	0.4	9.1	7.5	47.7	38.1	84.0	1.2
(110)	2	-1.58	6.9	13.5	13.9	3.1	19.9	10.5	1.3	tr	0.04	10.1	20.8	66.0	34.3	99.9	2.0
<i>n</i> (110) – (100)																	
(650)	6	-1.59	10.5	16.2	14.5	2.5	16.2	10.9	0.8	tr	0.06	6.1	20.6	64.8	41.2	98.4	1.5
(320)	3	-1.52	52.4	13.7	5.4	5.3	3.2	6.5	0.6	0.3	0.4	5.8	4.8	29.5	71.5	98.4	0.3
(210)	2	-1.52	64.0	13.4	2.2	7.0	0.9	6.6	0.6	0.2	0.5	5.5	0.7	22.9	79.6	101.6	0.2

Electrolyte solution: 0.1 M KHCO₃; current density: 5 mA cm⁻². MeD: acetaldehyde; EtOH: ethanol; PrD: propionaldehyde; AlOH: allyl alcohol; PrOH: propanol. C₂+ contains all the substances which have more than two carbon atoms. The gas total contains all the gaseous products other than H₂; tr: <0.05%.

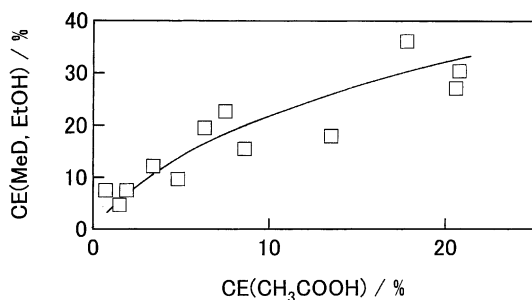


Fig. 6. Correlation of the sum of the current efficiency of CH_3CHO and $\text{C}_2\text{H}_5\text{OH}$ with that of CH_3COOH for $\text{Cu}(\text{S})\text{-}[n(111) \times (111)]$ and $\text{Cu}(\text{S})\text{-}[n(110) \times (100)]$ electrodes.

Fig. 7 illustrates another correlation of $\text{CH}_3\text{CHO} + \text{C}_2\text{H}_5\text{OH} + \text{CH}_3\text{COOH}$ versus CH_4 for the two crystal orientation series. A good correlation curve is obtained. We examined a similar correlation for the other series of the electrodes, but no such correlation was observed for the others.

3.5. Comparison of the product distribution between $\text{Cu}(\text{S})\text{-}[n(111) \times (111)]$ and $\text{Cu}(\text{S})\text{-}[n(111) \times (100)]$ series

The two crystal orientations have the surfaces of similar atomic configuration; the structure of the step site is different between the two. However, the product distribution from both the series differs to a great extent. If one compares the product distribution of the two series at the same n value in Tables 3 and 4, CH_4 formation in $\text{Cu}(\text{S})\text{-}[n(111) \times (111)]$ series

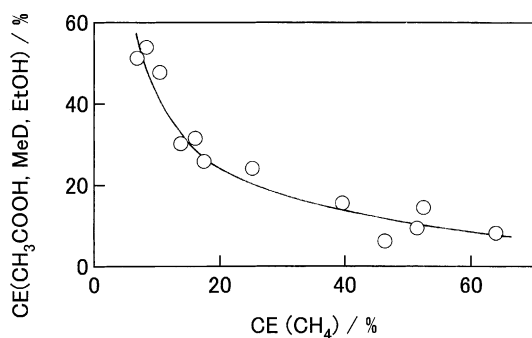


Fig. 7. Correlation of the sum of the current efficiency of CH_3COOH , CH_3CHO and $\text{C}_2\text{H}_5\text{OH}$ with that of CH_4 for $\text{Cu}(\text{S})\text{-}[n(111) \times (111)]$ and $\text{Cu}(\text{S})\text{-}[n(110) \times (100)]$ electrodes.

is much lower than in $\text{Cu}(\text{S})\text{-}[n(111) \times (100)]$ series. CH_3CHO , $\text{C}_2\text{H}_5\text{OH}$ and CH_3COOH formation in $\text{Cu}(\text{S})\text{-}[n(111) \times (111)]$ series is much higher than in $\text{Cu}(\text{S})\text{-}[n(111) \times (100)]$ series. This fact and the correlations shown in Figs. 6 and 7 suggest that some precursor leading to form CH_3COOH may be favorably formed at the (111) step sites on $\text{Cu}(\text{S})\text{-}[n(111) \times (111)]$ series. CH_3COOH may be further reduced sequentially to CH_3CHO and $\text{C}_2\text{H}_5\text{OH}$.

3.6. Unique electrocatalytic property of $\text{Cu}(110)$

$\text{Cu}(110)$ shows a unique electrocatalytic activity in the formation of CH_3CHO , $\text{C}_2\text{H}_5\text{OH}$ and CH_3COOH among $\text{Cu}(\text{S})\text{-}[n(111) \times (111)]$ series; the sum of CH_3CHO , $\text{C}_2\text{H}_5\text{OH}$ and CH_3COOH for $\text{Cu}(110)$ ($n = 2$) is significantly higher than that for $\text{Cu}(331)$ ($n = 3$) as shown in Table 4. (110) provides closely adjacent (111) step lines. Such adjacent (111) step lines may synergistically promote the formation of the intermediate species for CH_3COOH , CH_3CHO and $\text{C}_2\text{H}_5\text{OH}$, and simultaneously suppress the formation of CH_4 .

(311) , expressed in $2(111) - (100)$ or $2(100) - (111)$, has two adjacent step lines, i.e. (111) step lines and (100) ones. The product distribution of the (311) differs significantly from the (110) ($=2(111) - (111)$) which is composed of adjacent (111) step lines. The (311) gives very low yields of CH_3CHO , $\text{C}_2\text{H}_5\text{OH}$ and CH_3COOH with relatively high yield of CH_4 as shown in Table 3. Thus, the (111) step sites adjacent to (111) structure will favor the formation of a precursor leading to CH_3COOH .

The $\text{Cu}(\text{S})\text{-}[n(110) \times (100)]$ series provides adjacent (111) step lines the length of which is limited by the presence of (100) step lines. Table 4 shows that the formation of CH_3CHO , $\text{C}_2\text{H}_5\text{OH}$ and CH_3COOH decreases at n below 3. Thus, the unique electrocatalytic property of (110) structure appears for the (111) step lines with a certain length.

4. Conclusion

Electrocatalytic activity of copper single crystal electrodes in the electrochemical reduction of carbon dioxide were compared using the following series of the crystal orientations; $\text{Cu}(\text{S})\text{-}[n(100) \times (111)]$,

Cu(S)-[$n(100) \times (110)$], Cu(S)-[$n(111) \times (100)$], Cu(S)-[$n(111) \times (111)$] and Cu(S)-[$n(110) \times (100)$]. The electrolyses were conducted in 0.1 M KHCO_3 aqueous solution at constant current density 5 mA cm^{-2} . The reaction selectivity varied greatly with the crystal orientation. The electrocatalytic activity of C_2H_4 formation on Cu(S)-[$n(100) \times (111)$] and Cu(S)-[$n(100) \times (110)$] is further activated by introduction of a certain amount of the step atoms. Gaseous products are predominantly formed at Cu(S)-[$n(111) \times (100)$]. The CH_4 formation is enhanced in this series. Thus the $\text{C}_2\text{H}_4/\text{CH}_4$ value in the current efficiency varied in two orders of magnitude. The Cu(S)-[$n(111) \times (111)$] electrodes give high amount of C_2+ substances, and the (110) electrode derived from Cu(S)-[$n(111) \times (111)$] uniquely produces high yield of CH_3COOH , CH_3CHO and $\text{C}_2\text{H}_5\text{OH}$. The (111) step line adjacent to (111) structure may be effective for formation of the precursor for CH_3COOH . The precursor may be sequentially reduced to CH_3COOH , CH_3CHO and $\text{C}_2\text{H}_5\text{OH}$.

Acknowledgements

A part of the experimental works were conducted by R. Miura. This work was supported by Research Institute of Innovative Technology for the Earth of Japan (RITE), New Energy and Industrial Technology Development Organization (NEDO), and the Grant-in-Aid for Scientific Research (12650805) from

the Ministry of Education, Science and Culture of Japan.

References

- [1] R.I. Masel, Principles of Adsorption and Reaction on Solid Surfaces, Wiley, New York, 1996, p. 458.
- [2] N. Hoshi, S. Kawatani, M. Kudo, Y. Hori, J. Electroanal. Chem. 467 (1999) 67.
- [3] B.N. Nikolic, H. Huang, D. Gervasio, A. Lin, C. Fierro, R.R. Adzic, E. Yeager, J. Electroanal. Chem. 295 (1990) 415.
- [4] N. Hoshi, Y. Hori, Electrochim. Acta 45 (2000) 4263.
- [5] N. Hoshi, T. Uchida, T. Mizumura, Y. Hori, J. Electroanal. Chem. 381 (1995) 261.
- [6] N. Hoshi, H. Ito, T. Suzuki, Y. Hori, J. Electroanal. Chem. 395 (1995) 309.
- [7] N. Hoshi, M. Noma, T. Suzuki, Y. Hori, J. Electroanal. Chem. 421 (1997) 15.
- [8] Y. Hori, K. Kikuchi, S. Suzuki, Chem. Lett. (1985) 1695.
- [9] Y. Hori, K. Kikuchi, S. Suzuki, Chem. Lett. (1986) 897.
- [10] K.W. Frese Jr., in: B.P. Sullivan, K. Krist, H.E. Guard (Eds.), Electrochemical and Electrocatalytic Reactions of Carbon Dioxide, Elsevier, Amsterdam, 1993, p. 191.
- [11] Y. Hori, H. Wakebe, T. Tsukamoto, O. Koga, Surf. Sci. 335 (1995) 258.
- [12] Y. Hori, I. Takahashi, O. Koga, N. Hoshi, J. Phys. Chem. B 106 (2002) 15.
- [13] I. Takahashi, O. Koga, N. Hoshi, Y. Hori, J. Electroanal. Chem. 533 (2002) 135.
- [14] Y. Hori, O. Koga, H. Yamazaki, T. Matsuo, Electrochim. Acta 40 (1995) 2617.
- [15] O. Koga, T. Matsuo, N. Hoshi, Y. Hori, Electrochim. Acta 44 (1998) 903.
- [16] Y. Hori, O. Koga, T. Watanabe, T. Matsuo, Electrochim. Acta 44 (1998) 1389.